CloudSat snowfall estimates over Antarctica and the Southern Ocean: An assessment of independent retrieval methodologies and multi-year snowfall analysis

CloudSat snowfall estimates over Antarctica and the Southern Ocean: An assessment of independent retrieval methodologies and multi-year snowfall analysis

Lisa Milani[a,*], Mark S. Kulie[b], Daniele Casella[a], Stefano Dietrich[a], Tristan S. L'Ecuyer[c], Giulia Panegrossi[a], Federico Porcù[d], Paolo Sanò[a], Norman B. Wood[e]

[a] *Institute of Atmospheric Sciences and Climate, National Research Council (ISAC-CNR), Via Fosso del Cavaliere 100, Rome 00133, Italy*

[b] *Department of Geological and Mining Engineering and Sciences, Michigan Technological University, 1400 Townsend Drive, Houghton, MI 49931, USA*

[c] *Department of Atmospheric and Oceanic Sciences, University of Wisconsin-Madison, 1225 W. Dayton St., Madison, WI 53706, USA*

[d] *Department of Physics and Astronomy, University of Bologna, Bologna, Italy*

[e] *Space Science and Engineering Center, University of Wisconsin-Madison, 1225 W. Dayton St., Madison, WI 53706, USA*

Abstract

CloudSat spaceborne radar snowfall retrievals using two different methodologies – the 2C-SNOW-PROFILE (2C- SNOW) CloudSat product and the combined Kulie and Bennartz (2009) technique with the Hiley et al. (2011) reflectivity (Z) to snowfall rate (S) conversion (KBH) - are compared over Antarctica and surrounding Southern Ocean environments. KBH algorithm sensitivity tests are performed to demonstrate how retrievals are affected by algorithm assumptions (e.g., vertical reflectivity continuity test, the choice of near surface bin used to make surface snowfall rate retrievals, and temperature filters). These algorithm components are found to be detri- mental to snowfall detection over this region by significantly reducing the snowfall population compared to 2C- SNOW, especially over ocean regions prone to ERA-interim indicated convective snow. After accounting for key algorithm differences, 2C-SNOW mean annual snowfall rates are systematically higher than KBH due to the Z-S relationship adopted. Spatial annual mean snowfall accumulation differences between the two datasets are minimized over interior Antarctica, but large differences are observed over the ocean. 2C-SNOW Z-S relation- ships for all snowfall events ($Z = 10.9 \, S^{1.3}$), over ocean and sea ice ($Z = 8.2 \, S^{1.3}$), escarpments and Antarctic coastal areas - below 2000 m a.s.l. ($Z = 6.7 \, S^{1.4}$), and Antarctic plateau - above 2000 m a.s.l. ($Z = 5.5 \ \, S^{1.6}$) are also derived. A multi-year 2C-SNOW mean annual snowfall analysis is also provided, and comparisons with ERA-Interim snowfall datasets show similar spatial patterns, but magnitude differences over oceans are observed. A monthly 2C-SNOW and acoustic depth gauge analysis is provided to demonstrate qualitative trends in snowfall accumulation between the respective datasets.

1. Introduction

Accurately quantifying atmospheric parameters in polar regions is essential for better understanding the global hydrologic cycle and en- ergy budget, especially since certain higher latitude areas have ex- perienced accelerated warming trends in recent years (Bromwich et al., 2013; Nicolas and Bromwich, 2014; Clem and Fogt, 2015). There are, however, numerous challenging aspects to characterizing important weather and climate parameters and their concomitant variability in polar regions (Lubin and Massom, 2006). For example, surface pre- cipitation that usually occurs in the solid phase at high latitudes is a particularly vexing parameter that often demonstrates extreme spatiotemporal variability. Surface snowfall –which is often very light in polar climates - is also very difficult to detect and quantify using sparse ground measurements and current satellite observations (e.g., Bromwich, 1988; Kulie and Bennartz, 2009; Palerme et al., 2014).

Antarctica and its associated ice shelves has received sustained scientific attention for many decades, but surface precipitation char- acterization is hindered by a sparse observational network that relies on many different collection tools and methods (e.g., precipitation gauges, snow pits, acoustic instruments, snow stakes, etc.) that measure dif- ferent frozen precipitation properties with varying sensitivities. Each respective method also contains observational errors that are some- times difficult to quantify (e.g., Eisen et al., 2008; Knuth et al., 2010).

Accurate ground-based snowfall measurements also require constant and effective instrument maintenance over the long durations needed to study precipitation. Data, instruments and techniques used affect and make difficult the spatial interpolation of such sparse data (Arthern et al., 2006; Eisen et al., 2008). Preliminary results from a recently established experimental site indicate that light snowfall rates dominate the snowfall rate spectrum, but these prevalent light snow events are interspersed with rare heavy snowfall events that contribute significantly to the surface mass balance (Gorodetskaya et al., 2014, 2015). Further long-term ground-based observational studies are needed to sample widely varying Antarctic environments.

The scientific community has relied heavily on climate models to study Antarctic Surface Mass Balance (SMB) and in particular pre- cipitation among the various SMB components. Modeled precipitation fields have provided important climatic context to assess annual pre- cipitation trends (Bromwich et al., 2011). The polar MM5 model (Guo et al., 2003) for example has been used to characterize the spatio- temporal distribution of Antarctic snowfall and blowing snow

(Bromwich et al., 2004). The RACMO2 regional climate model and its updated physics schemes have also improved Antarctic surface energy balance and precipitation estimates (Van Wessem et al., 2014). Numerical model validation, however, is hampered by the aforementioned sparse ground-based observations. Large biases and relatively high errors also affect numerical model and ground-based measurement comparisons (Genthon and Krinner, 2001; Grazioli et al., 2017). Satellite precipitation products, even with known uncertainties and limitations, provide valuable independent datasets to evaluate models on a more spatially and temporally extensive basis compared to ground measurements (Palerme et al., 2017; Tapiador et al., 2017).

Passive microwave spaceborne sensors on Low Earth Orbiting (LEO) satellites have been successfully utilized to estimate precipitation at higher latitudes (e.g., Huffman et al., 2007). However, light and solid precipitation detection over Antarctica is difficult due to the highly emissive snow/ice surface background combined with low ice water paths in weaker snowfall-producing clouds (Kongoli et al., 2015; You et al., 2017). Several studies have theoretically assessed high frequency passive microwave channels' ability to detect and retrieve snowfall (e.g., Skofronick-Jackson and Johnson, 2011; Munchak and Skofronick- Jackson, 2013). High frequency channels (> 150 GHz) show promise, but the signal is extremely sensitive to highly varying cloud micro- physical composition (e.g., Kulie et al., 2010; Johnson et al., 2012), and environmental conditions (e.g., humidity and background surface, as evidenced in Panegrossi et al., 2017). Passive microwave radiometry using water vapor absorption band channels near 183 GHz or brightness temperature differences between vertically and horizontally polarized high frequency channels to eliminate background surface signals also offer promise (e.g., Surussavadee and Staelin, 2009; Laviola and Levizzani, 2011; Gong and Wu, 2017), but these techniques are com- plicated by Antarctica's dry atmospheric conditions. Dedicated studies to demonstrate the veracity of these techniques for accurate snowfall retrievals in the polar regions are currently lacking. Since upwelling microwave radiation is extremely sensitive to surface snow or ice morphology, an alternative approach evaluated snowfall occurrence by studying surface radiative property fluctuations (Bindschadler et al., 2005). This method, however, does not provide quantitative snowfall estimates. Snowfall detection and retrieval advances are expected with the Global Precipitation Measurement (GPM) mission Core Observatory (CO) (Hou et al., 2014). However, GPM-CO's orbital range between 65°S and 65°N does not enable the use of such a valuable spaceborne observational platform for Antarctica snowfall research.

The most useful tool for snowfall remote sensing at high latitudes is currently the Cloud

Profiling Radar (CPR) onboard the CloudSat sa- tellite launched in 2006 (Stephens et al., 2008). The W-band, nadir- viewing CPR provides radar reflectivity profiles, allowing physical re- trievals of cloud and precipitation (Stephens et al., 2002; Liu, 2008), and, after adopting relevant cloud microphysical assumptions, quantitative snowfall rate estimates (Hudak et al., 2008; Liu, 2008; Kulie and Bennartz, 2009; Wood et al., 2013). After CloudSat's first operational year, global snowfall studies were published to illustrate CloudSat's unique snowfall observational capabilities (Liu, 2008; Hiley et al., 2011). Because of its high sensitivity to light precipitation, several studies use CloudSat products to assess snowfall detection cap- abilities of other sensors (Casella et al., 2017; Panegrossi et al., 2017). Multi-year CloudSat snowfall studies with extensive Antarctic region snowfall analyses have also been undertaken in recent years (e.g., Boening et al., 2012; Palerme et al., 2014; Kulie et al., 2016; Kulie and Milani, 2018). A CloudSat snowfall retrieval product has also been released to accommodate global snowfall studies. This product – named 2C-SNOW-PROFILE – provides "near surface" and vertical snowfall rate retrievals for each CPR profile (Wood et al., 2013).

Similarly to Palerme et al. (2014), this study uses a multi-year dataset of CloudSat snowfall retrievals to investigate precipitation char- acteristics over Antarctica, including spatial distributions of annual snow amounts. Unlike Palerme et al. (2014), we also analyze oceanic regions surrounding Antarctica. Furthermore, we analyze and interpret systematic differences between two CloudSat snowfall retrieval algorithms. The spaceborne results are also compared to ERA-Interim (Dee et al., 2011) reanalysis data and local ground-based Acoustic Depth Gauge (ADG) observations.

The main goals of this study are:

I. Evaluate the CloudSat 2C-SNOW-PROFILE and Kulie and Bennartz (2009) snowfall retrievals to determine if systematic differences exist in the pan-Antarctic and Southern Ocean region. Possible causes of algorithm differences are also explored.

II. Compare CloudSat snowfall retrievals with ERA-Interim (ERA-I) reanalysis and ground-based snow accumulation estimates.

III. Provide a multi-year snowfall "climatology" in the region south of

60°S (including both Southern Ocean and continental Antarctica) using the 2C-SNOW-PROFILE dataset.

2. Data and algorithms

2.1. CloudSat products and algorithms

The CloudSat research satellite's CPR provides critical observations to understand the role of clouds in the climate system (Stephens et al., 2008). CloudSat flies in the Afternoon, or A-Train, satellite formation, providing radar reflectivity factor (hereafter referred to as reflectivity (Z)) profiles of the lowest 30 km of the atmosphere (Tanelli et al., 2008). CPR is a nadir-pointing radar operating at 94GHz frequency (W-band), with a 240 m vertical resolution bin and a ~1.7 × 1.4 km^2 spatial footprint. The bins near the surface could contain anomalously large reflectivity values, most likely related to ground clutter contamination (Marchand et al., 2008; Tanelli et al., 2008). Depending on the surface type and on the methodology used to estimate precipitation, a defined number of those bins are excluded from the algorithms (see Sections 2.1.1 and 2.1.2 for further details) and a "Near Surface Bin" (NSB) is then defined as the lowest bin actually considered in the algorithms (Liu, 2008), with an elevated height ranging from about 720 m to about 1440 m depending on the algorithm and the surface. This "blind zone" can adversely affect CloudSat surface snowfall estimates in Antarctica depending on precipitation regime (Maahn et al., 2014).

The CPR can experience gaseous and hydrometeor attenuation, al- though Antarctica's drier, colder environment generally limits W-band attenuation effects. The CPR's sensitivity (around −29 dBZ minimum detectable signal) is sufficient to observe light precipitation and most cloud structures (Haynes et al., 2009). The CPR's sensitivity and orbital range (between 81ºN/S latitude) allow it to effectively detect and retrieve snowfall distribution and intensity (Liu, 2008; Kulie and Bennartz, 2009; Hiley et al., 2011; Kulie et al., 2016; Behrangi et al., 2016; Kulie and Milani, 2018). Previous studies indicate that CloudSat snowfall product accuracy compares favorably with limited ground- based observations (Matrosov et al., 2008; Hudak et al., 2008).

This study considers almost five years of CloudSat CPR data (July 2006 to December 2010). This period is hereafter referred to as the Observing Period (OP). This OP contains a 560 orbit observational gap between 7 December 2009 to 16 January 2010 due to CPR battery problems. CPR observations in the Southern Hemisphere south of 60°S (hereafter Antarctic Region) are selected for this study. The CPR observations are further processed into 1° by 1.5° latitude/longitude grid boxes. The CPR daily overpass frequency for each grid box is between

0.3 and 1.3 over continental Antarctica. Oceanic grid boxes, on average, receive 1 overpass every 3 to 10 days.

CPR reflectivity profiles and data navigation/geolocation fields from the GEOmetrical PROfile (2B-GEOPROF) product (Mace, 2007) are used in this study. A 2B-GEOPROF data quality flag is also used to identify potentially corrupt observations, and only high quality profiles are considered.

The CloudSat SNOW PROFILE (2C-SNOW-PROFILE) product (Wood et al., 2013) provides NSB snowfall rate retrievals. These products are "global" products with no particular retrieval adaptation applied to the Antarctic environment. Additionally, the European Centre for Medium- Range Weather Forecasts (ECMWF)- Auxiliary (AUX) product (Partain, 2007) is used, where the ECMWF 2 m temperature (2mT) and other ancillary modeled state variables are interpolated to CPR observations.

2.1.1. *Kulie and Bennartz (2009) snowfall rate retrieval algorithm*

One snowfall retrieval algorithm employed over Antarctica is based on the Kulie and Bennartz (2009) technique using the Hiley et al. (2011) Z-S relationship (hereafter referred to as KBH). The Kulie and Bennartz (2009) technique considers precipitating snow profiles as CPR observations with NSB (defined for Kulie and Bennartz (2009) as the 6th bin from the ground – about 1440 m – independently of the surface type) Z exceeding −15 dBZ, and with a continuous vertical Z layer above −15 dBZ in at least 5 contiguous bins. This ad hoc vertical Z continuity test is implemented to mitigate CPR profiles infected by ground clutter. Only profiles with ECMWF-AUX 2mT lower than 0°C are considered in order to avoid profiles with wet snow or mixed phase precipitation. Snowfall rate (S) is then computed for the Kulie and Bennartz (2009) technique by applying a Z-S relationship to the NSB Z ($Z = a\ S^{b}$, where Z contains units of $[mm^{6}\ m^{-3}]$ and S is the water equivalent snowfall rate $[mm\ h^{-1}]$). The Z-S relationships are based on simulated radar scattering properties (Liu, 2008; Hong, 2007; Surussavadee and Staelin, 2009) combined with a temperature-dependent ice particle size distribution parameterization (Field et al., 2005). Hiley et al. (2011) studied the sensitivity of the Kulie and Bennartz (2009) technique to the choice of key parameters, such as the depth of the vertical continuity test, Z thresholds, NSB among others. A variety of snowflake habit dependent *a* and *b* coefficient values in the Z-S formula are summarized by Hiley et al. (2011). Bromwich (1988) reports that columns, bullets, and column/bullet aggregates comprise most Antarctic precipitation at a handful of sites. However, despite the increment of microphysical

properties measurements collected over many Antarctic observation sites (Grazioli et al., 2017; Souverijns et al., 2017), it is still extremely difficult to determine an optimal *Z*-S relationship without a network able to provide solid precipitation microphysical information over the entire Antarctic continent and the surrounding ocean regions. We therefore applied static averaged *a* and *b* values from the 20 *Z*-S relationships derived by Hiley et al. (2011) to the KBH algorithm:

$$Z = 21.6 \, S^{1.2} \hspace{3cm} (1)$$

Hiley et al. (2011) also presented upper and lower bounding Z-S relationships as an important uncertainty estimate caused by varying snowfall microphysical composition. Results from these Z-S uncertainty estimates are not shown in this study since the average Z-S relationship compares most favorably to independent estimates from ERA-Interim (not shown in this study).

The NSB definition is relevant over Antarctica for two reasons: 1) Eastern Antarctica coastal areas are rugged with highly complex terrain and thus ground clutter could be problematic (Fig. 1a); 2) local snow- pack increases without contributions from precipitating snow can be caused by horizontal transport of snow from strong low-level winds (Li and Pomeroy, 1997). Following Kulie and Bennartz (2009), another test is applied on the CPR NSB to account for instances when the Digital Elevation Model (DEM) may not properly resolve the surface height in complex terrain. An additional ground clutter correction is then ap- plied. 20 dBZ is considered the theoretical upper bound for Z not as- sociated with clutter. 6th bin Z values exceeding this threshold are unlikely due to precipitation and their value cannot be considered re- liable for snowfall estimates. Under these circumstances the retrieval algorithm uses the 8th CPR bin instead of the 6th bin. Vertical layer continuity is also required, as previously described. The snowfall rate computed from the 8th bin Z is assigned to these profiles. In Fig. 1b, the normalized frequency of Z, corrected for ground clutter contamination, calculated either for the 6th bin or the 8th bin (in case Z at the 6th bin exceeding 20 dBZ), and the normalized distribution of the only 6th bin Z exceeding 20 dBZ are respectively shown in black and red lines.

"Contaminated" bin counts are very low (around 10^{-5} of the total), but the extremely high snowfall rates associated with these observations significantly impact mean precipitation rates. These intense snowfall rates indicate probable ground clutter contamination, including ground

clutter that can be embedded within legitimate precipitating profiles. Kulie and Bennartz (2009), in fact, highlight embedded ground clutter within deeper precipitating systems over Greenland (please consult Kulie and Bennartz (2009) Fig. 7 for further details). Further algorithm improvements are necessary to flag and mitigate such ground clutter contamination. An updated DEM that is expected to be incorporated into the next CloudSat product suite release might also improve near surface bin designation and reduce adverse clutter effects. Within the OP, about 0.28% of the observations over the whole Antarctic Region are corrected due to this screening process. This value increases to 2.57% for land surfaces with elevations below 2000 m. Sensitivity tests to various KBH algorithm assumptions to accommodate 2C-SNOW- PROFILE comparisons are presented in Section 3.

2.1.2. *CloudSat 2C-SNOW-PROFILE product*

The CloudSat snow profile product (2C-SNOW-PROFILE Release R04, hereafter 2C-SNOW) provides snowfall rate profiles and near- surface snowfall rate (Wood et al., 2013; Palerme et al., 2014). The product's retrieval algorithm minimizes differences between observed and simulated reflectivity profiles by varying snow microphysical properties subject to temperature-dependent a priori constraints on those properties. This approach leads to snowfall rates that depend on Z in a way that varies with both the structure of the observed reflectivity profile and with temperature. 2C-SNOW, similar to KBH, does not use the likely contaminated lowest bins directly above ground level. The NSB is defined in the 2C-SNOW product as the 3rd (5th) bin above the surface over ocean without sea ice, or over inland water (over land, sea ice, or unknown surface) profiles at 720 m (1200 m) above the surface. A -15 dBZ Z threshold is also applied to the NSB to include a profile as likely snowing. Retrieval results are used to calculate water contents and snowfall rates, then the snowfall rate at the NSB is assumed to be the snowfall rate at the surface. Retrievals are only performed when the melted mass fraction of the snow reaching the surface is estimated to be < 0.1; in practice, this means that retrievals are performed when the temperature in the NSB is less than about 1.5 °C. A number of studies (Palerme et al., 2014; Kulie et al., 2016; Cooper et al., 2017; Kulie and Milani, 2018) provide more detailed information about other aspects of the algorithm. 2C-SNOW also provides the snow_retrieval_status (SRS) flag as further quality control information. The SRS bit 3 binary value activates for situations when the snow layer base snowfall rate substantially exceeds the snowfall rate in the bin immediately above, thus indicating ground clutter effects, shallow

precipitation, or partially melted snow. These profiles should be used with caution. Under these circumstances, 2C-SNOW retrievals for the bin above the NSB are used. The SRS flag was not applied in previous CloudSat Antarctica snowfall studies and may contain localized snowfall maxima due to clutter in severe Antarctica topography.

After investigating the SRS flag distribution over the Antarctic ice sheet and Southern Ocean, profiles over land were found to contain increased SRS bit 3 activity that indicate possible surface clutter (Fig. 1c). Over ocean points may indicate an extremely shallow precipitation. Both situations are corrected using the snowfall rate value from the bin located immediately above the NSB. The normalized Z frequency used in the 2C-SNOW product retrieval is shown (black) in Fig. 1d, together with the normalized count of profiles marked as possible ground clutter (red). Similar to the KBH algorithm, the possible ground clutter count is also only $\sim 10^{-5}$ of the total profiles, but this low population of CPR observations affects mean annual snowfall rates. The annual mean snowfall rate decreases 1.2% over Antarctica after applying the ground clutter correction, but > 9.0% if land regions below 2000 m are only considered.

2.2. Ground data: acoustic depth gauges

Over Antarctica, there is a lack of systematic measurements of precipitation, while operational weather stations are often equipped with instruments for SMB measurement (Eisen et al., 2008). Among these, the Acoustic Depth Gauges (ADG) measure the changing distance from the instrument to the snow-covered surface, and have been used to study the influences of precipitation and horizontal snow transport on surface accumulation (Knuth et al., 2010). ADG-measured snow accumulations are influenced by many factors besides precipitation. Blowing snow, hoar frost deposition, surface sublimation, snowdrift sublimation, snowpack settling and compaction, and meltwater can all alter snowpack height changes (Knuth et al., 2010; Li and Pomeroy, 1997). In this work, we use ADG measurements to perform qualitative comparison with the snow accumulation values estimated by CPR precipitation products.

This study uses data from five University of Wisconsin-Madison Automatic Weather Station ADG shown in Fig. 2 (Knuth et al., 2010). Observations from these ADGs are analyzed for the last 2 years of the OP. 10-minute ADG accumulations are processed on a monthly basis by considering the ADG distance measurement difference at the end and beginning of each month.

The distance at the beginning (end) of each month is computed as the mean distance over the first (last) five days of the month and the last (first) five days of the previous (following) month. After performing a simple quality control test that identifies outlier observations (unreasonably large 10-minute ADG distance values), the monthly distance variation was calculated. A positive (negative) ADG distance variation for one month indicates a decrease (increase) of the monthly accumulated snow. A negative monthly ADG distance variation value is therefore interpreted as a positive monthly accumulation whereby the average surface snow accumulation at the end of the month exceeds the beginning of the month.

3. Results

3.1. KBH vs 2C-SNOW comparison

3.1.1. Near surface bin (NSB) and vertical continuity test (CT)

This subsection focuses on two snowfall rate algorithm assumptions that cause discrepancies between KBH and 2C-SNOW – the KBH vertical reflectivity continuity test (CT) required to include a CloudSat profile as a snow event and near surface bin (NSB) designation. Fig. 3 illustrates that the sensitivity of the snowfall rate distribution to the CT in the Antarctic Region is relatively minor, with only very small differences between the KBH snowfall rate distributions with (red) and without (blue) applying the CT. Fig. 3 indicates a slightly reduced snowfall rate occurrence at high values when the CT is applied. Even though the snowfall rate distributions are very similar when the CT is eliminated, Antarctic Region snowfall cases occurrences increase by 70.6% (about ten million additional snowfall detections) when the CT criterion is not applied to identify a snowfall event. These results indicate that very light snowfall rates are associated with probable shallow snowfall events in this region. This difference in snowfall population counts due to the CT shows similar trends as the more limited dataset analyzed by Hiley et al. (2011). The abrupt 3.5 mm h^{-1} cutoff in the original KBH algorithm (with and without CT) is due to the ground clutter filter (Z > 20 dBZ are avoided).

To better facilitate 2C-SNOW and KBH comparisons, the KBH sen- sitivity to NSB is assessed, whereby the KBH NSB is forced to adopt the lower 2C-SNOW NSB (the 3rd (5th) CPR bin above the surface over water (land)). The ad hoc maximum Z threshold (20 dBZ) from KBH is also relaxed to allow direct 2C-SNOW comparisons. The KBH snowfall rate distribution

displays a higher number of elevated snowfall rate occurrences when a lower NSB is used ("KB low" green line in Fig. 3). These normalized distribution differences are accentuated when the lower NSB is used and the CT is not applied ("KB low noCT" pink line), thus implying systematically increasing radar reflectivity values at CPR bins located closer to the surface. Fig. 3 also highlights a final distinctive feature. The optimal KBH comparison from a methodological perspective (no CT, lower NSB) displays a much different snowfall rate normalized distribution compared to 2C-SNOW. 2C-SNOW shows consistently higher snowfall rate counts over most of the snowfall rate spectrum, although the distribution is very similar for lighter snowfall events. The systematic snowfall rate distribution difference between the altered KBH and 2C-SNOW algorithms is thus related to other algorithm differences that will be explored further in later sections.

The NSB used for spaceborne snowfall rate retrievals, considered without applying the CT, are therefore deemed to be critical algorithm decisions since the sensitivity tests shown in Fig. 3 reflect large vertical reflectivity gradients in many snowfall events. Shallow snowfall events are especially vulnerable to both the KBH NSB designation and CT. Fig. 4, highlights the KBH algorithm assumption sensitivity by showing mean annual snowfall rate difference spatial maps for the 5 year OP (expressed in mm yr^{-1}). The differences indicated in Fig. 4a–c are directly attributed to the CT and NSB choice. The largest differences are observed over the Southern Ocean at lower latitudes between ~60–180°W and ~30–150°E longitude. Respective annual snowfall rate differences due to CT (Fig. 4a) and NSB designation (Fig. 4b) and combined effects (Fig. 4c) show regions where the mean annual snowfall rate differences exceeds 50% (relative difference) on the periphery of the domain. Interior Antarctica shows increases in the mean annual snowfall rate magnitude, but the northern oceanic regions show much larger increases compared to interior Antarctica. Note, however, that interior Antarctica generally receives reduced annual snowfall amounts than the ocean regions, so the small increases in Fig. 4c are associated with relative percentage differences exceeding 200%.

CloudSat studies have shown that convective snow over this oceanic region is typically associated with shallower cloud structures (Kulie et al., 2016; Kulie and Milani, 2018). Shallow convective snowfall dominates (> 50% occurrence) from about −60° equatorward and nimbostratus (synoptic-scale systems) dominate from about −60° poleward (Fig. 8 in Kulie et al., 2016). In order to connect the con- vective nature of the snowfall missed by KBH applying the CT and with the NSB choice, Fig. 4d shows the mean yearly cumulated snowfall attributed to

convective snow from ERAeI. Modeled convective snowfall clearly increases in magnitude from about $-70°$ and equatorward. This convective field includes both shallow convection and deep convection, although shallow convective snow is presumed to dominate based on CloudSat analyses. The snowfall rate difference between the 3rd (or 5th over land) and the 6th bins is shown in Fig. 4c. If a non-zero snowfall rate is given for the 3rd bin and not for the 6th, it means that the snowing layer is shallow and between 720 m and 1440 m. We discovered that this difference is higher over the regions labeled as shallow convective from Kulie et al. (2016) and also from Kulie and Milani (2018). Kulie and Milani (2018) Fig. 1c specifically shows the Southern Hemisphere shallow convective mean snowfall rate - the magnitude and pattern are comparable with the differences shown in Fig.4c. As a consequence, the differences in Fig. 4c can be attributed to the shallow convective snowfall missed from the restrictive conditions imposed by KBH. Further, the difference magnitude corresponds to the magnitude of the mean shallow convective snowfall for that region according to Kulie and Milani (2018). The mean ERA-I convective snow accumulation shown in Fig. 4d also has the same pattern and magnitude as Fig. 4c. We therefore conclude that the ERA-I convective field, even if both shallow and deep convection are included, shows almost only shallow convective snow accumulation and compares favorably with the CloudSat observational dataset.

Fig. 4c also shows a narrow region along the Antarctic Peninsula coastline and other isolated coastal regions that are susceptible to KBH algorithm assumptions. ERA-I indicates reduced convective snow magnitudes in these regions, so convective snow is a less likely culprit to explain the CT and NSB sensitivity. Isolated ground clutter effects may inflate the differences shown in Fig. 4c over the Antarctic Peninsula, but further inspection of the CloudSat dataset is necessary to confirm this hypothesis. Interior Antarctica is relatively immune to the KBH algorithm assumptions.

3.1.2. Temperature filter

A final algorithm component (2mT) needs to be considered before KBH and 2C-SNOW results can be directly compared. As previously discussed, KBH utilized a 0°C 2mT threshold to consider precipitating CloudSat observations as dry snowfall events, even though 2°C delineates the 50% snow probability threshold based (Liu, 2008). The 2C- SNOW algorithm, however, allows CloudSat snowfall events to be as- sociated with 2mTs exceeding 0°C based on estimated particle melt fraction. The 0 °C threshold applied by KBH was adopted in an attempt to consider

dry snowfall cases that are more appropriately represented by the ice scattering models used in the study. This strict threshold, however, will lead to fewer snowfall events identified by KBH com- pared to the 2C-SNOW temperature restrictions. Fig. 5 indicates the percentage of CloudSat observations in the 5 year OP associated with 2 mT > 0°C. Peripheral Southern Ocean regions are more susceptible to KBH temperature restrictions since ~50–70% of all CloudSat observations between 60-120°W and north of ~65°S latitude are associated with T > 0°C. Regions between 120°E and 150°W also contain elevated T > 0°C occurrences. These same regions also contain frequent ERA-I convective snow (Fig. 4d), so the KBH CT and T thresholds combine to reduce the snowfall population. The 45°W to 105°E region generally experiences under 30% T > 0 °C frequency, with drastically reduced values closer to Antarctica. The northern Antarctic Peninsula straddles the elevated T > 0 °C percentage values near 60°W and experiences a relatively small percentage of above freezing temperatures. Fig. 5 confirms that ocean regions sur- rounding Antarctica are almost exclusively sensitive to KBH temperature thresholds, while Antarctica is not adversely affected by the same restrictions.

Fig. 6 shows snowfall rate distributions from the Antarctic region OP associated with 2C-SNOW (Fig. 6a) and the original and modified KBH (Fig. 6b–e) algorithms, including snowfall rate distributions partitioned by "warm" (T > 0 °C) and "cold" (T ≤ 0 °C) 2 mTs. The KBH "warm" results include all probable CloudSat precipitation events as- sociated with temperatures between 0 °C and 4 °C, so mixed or light rain events may be included in the distributions over the oceans. The 2C- SNOW algorithm "warm" category contains observations under about 2 °C based on the temperature criteria previously explained.

The 2C-SNOW snowfall rate distribution shown in Fig. 6a indicates that "warm" snowfall events comprise a lower percentage of the total snowfall in this region compared to the "cold" snowfall category. This result is not surprising given the influence of very cold temperatures in the latitudinal domain chosen for this study. The "cold" snowfall population also contains systematically higher snowfall rates than the "warm" category.

Fig. 6b–e illustrate the KBH snowfall rate distribution sensitivity to various methodological assumptions. The KBH "warm" category in each figure also highlights the potential population of snowfall events missed when a 0 °C temperature threshold is applied. However, under any methodological assumptions, as for 2C-SNOW, high rate snowfall events (> ~2.5 mm h^{-1}) are exclusively attributed to the "cold" snowfall population. Moreover, Fig. 6d-e show that the ~3 mm h^{-1} cutoff of the KBH original (Fig. 6b) and KBH with no CT (Fig. 6c) for the "cold"

category is completely avoided after lowering the NSB. Snowfall rate distributions are similar to 2C-SNOW, with maximum values ranging from 4 to 6 mm h^{-1} for lower NSB and lower with no CT assumptions, respectively.

3.1.3 Minimized 2C-SNOW and KBH differences

The first two subsections highlight a major issue to be considered: KBH and 2C-SNOW algorithm methodological differences need to be addressed before critical assessment exercises can be undertaken be- tween the respective algorithms. Figs. 3–6 suggest that the KBH algorithm employs more restrictive criteria for snowfall detection purposes, and these restrictions should be relaxed to include as many snowfall events as possible in the CloudSat snowfall dataset. Fig. 7 provides an optimal comparison between KBH and 2C-SNOW that minimizes algorithm differences due to surface temperature (only "cold" temperatures are used), NSB, and CT application (no CT applied). Fig. 7 shows large differences between the mean annual snowfall rate calculated by the 2C-SNOW and KBH algorithms over the extreme southern latitudes. These differences are due to Z-S relationships used by each algorithm, and we posit that the dynamic 2C-SNOW Z-S strategy may capture inherent microphysical differences between snowfall modes or regional snowfall differences. Fig. 7 illustrates where such differences are maximized, such as over-ocean regions influenced by synoptic-scale storms and/or with frequent convective snowfall events. Coastal Antarctic regions and ice sheets also exhibit differences, but differences are minimized compared to open ocean. The interior Antarctica differences are largely irrelevant, highlighting that the 2C-SNOW microphysical constraints yield a similar Z-S relationship as KBH in very cold Antarctic regions that experience predominantly light snowfall events. These regions are further highlighted in the next subsection.

3.1.3. Regional analysis by surface type

Fig. 8 shows 2C-SNOW and KBH modified algorithm snowfall rate distributions for all snowfall events over the domain. Regional differences partitioned by general surface type, ocean and sea ice, escarpments and Antarctic coastal areas (below 2000 m a.s.l.), Antarctic plateau (above 2000 m a.s.l.), hereafter ocean, < 2000 m, and > 2000 m, are also indicated. Note that Fig. 8a is similar to Fig. 3, but total counts are shown instead of normalized counts. Fig. 8 highlights surface type dependent differences between KBH CT and no CT applications, as well as KBH results with lower NSB designation to mimic 2C-SNOW (with or without CT).

The 2C-SNOW results (black) illustrate oceanic snowfall events dominating the total number of snowfall counts for lower snowfall rates. < 2000 m, after an initial steep gradient, becomes comparable to ocean for higher rates (> ~2 mm h^{-1}), although < 2000 m counts exceed ocean at the highest snowfall rates shown. > 2000 m counts are much lower than other surface types and are skewed to lighter snowfall rates. KBH results, using the same 2C-SNOW NSB designation and without a CT (pink line - "low noCT"), show the most consistency with 2C-SNOW results, although large regions of the KBH "low noCT" snowfall rate count spectrum are lower than 2C-SNOW. This trend is accentuated over the oceans and minimized over the > 2000 m, again highlighting the effect of different Z-S relationships used by each algorithm.

The various KBH sensitivity tests show very interesting trends over the different surface types and further highlight the effect of algorithm- specific snowfall event definitions. Over ocean surfaces (Fig. 8b), no substantial differences exist between various KBH algorithms below the ~3.5 mm h^{-1} snowfall rate level. The KBH "low" (green) and KBH "low noCT" (pink) exhibit some differences at the highest snowfall rates. The "low noCT" algorithm also captures an apparent shallow, intense snowfall mode more effectively than other KBH results.

Over < 2000 m surfaces (Fig. 8c), the original KBH algorithm (red) underestimates snowfall events relative to 2C-SNOW and modified KBH algorithms at ~ 2 mm h^{-1} and completely misses snowfall events over ~3.5 mm h^{-1}. The KBH "low noCT" results show the most pronounced departure from KBH original results, thus illustrating the impact of considering shallow snowfall events that are eliminated by the CT. Note that the higher snowfall rate populations over < 2000 m smoothly increase under these circumstances, thus indicating a legitimate shallow snow land enhancement or ground clutter contamination. Unlike the ocean distribution, the KBH "low noCT" counts exceed 2C-SNOW at the highest snowfall rates, thus further raising suspicion that ground clutter at least partially affects the KBH snowfall population over Antarctica.

Over the > 2000 m (Fig. 8d), the various KBH snowfall rate distributions display expected behavior similar to the < 2000 m distributions, although a slightly different behavior is noted between the CT versus no CT distributions compared to < 2000 m. The choice of NSB is the only distinction between these two methodologies, and this effect is small over the > 2000 m regions. The KBH "noCT" (blue) includes progressively more snowfall events than the KBH CT results, thus including more shallow snow or ground clutter effects. The KBH "low noCT" results (pink) produce the highest count of snowfall events at elevated snowfall rate values.

3.2. 2C-SNOW derived Z-S relationships

Fig. 9 illustrates joint distributions of CloudSat NSB reflectivity and 2C-SNOW snowfall rate retrievals for the same surface type categories shown in Fig. 8. The NSB reflectivities are, in this case, taken from the 2B-GEOPROF product and may slightly differ from the 2C-SNOW Z used to derive the snowfall rate, whereby 2C-SNOW models multiple scat- tering and attenuation effects. These effects, however, may counteract each other under most snowing conditions (Matrosov and Battaglia, 2009). Fig. 9 shows distinct differences in the regional Z-S relationships provided by the 2C-SNOW retrievals. Using a best fit through the data points indicated in Fig. 9, the 2C-SNOW Z-S relationship for all snow events in the domain is $Z = 10.9\ S^{1.3}$, which differs from the static Z-S relationship ($Z = 21.6\ S^{1.2}$) used in previous sections for the modified KBH algorithm. Note, however, that derived Z-S differences are evident when the CloudSat dataset is partitioned by surface type. Ocean ($Z = 8.2\ S^{1.3}$), < 2000 m ($Z = 6.7\ S^{1.4}$), and > 2000 m ($Z = 5.5\ S^{1.6}$) observations have significantly different derived Z-S relationships, partially driven by cloud microphysical properties constrained by regional temperature variability. These regional results highlight the in- creased uncertainty associated with using a globally invariant Z-S relationship, and indicate that methods that can allow Z-S to adjust to local conditions will provide better performance than methods with static Z-S relationships Ground validation datasets are admittedly needed, however, to confirm the veracity of the CloudSat Z-S relationships reported in this study (see Section 4 for further discussion of this topic). The more restrictive criteria of KBH on detecting and estimating snowfall, like temperature filter, NSB designation, CT and very conservative ground clutter filters discussed above, and the dynamic Z- S relationship of 2C-SNOW more adaptable to the local microphysical conditions, providing better performances than methods with static Z-S relationship, led us to consider 2C-SNOW for the following Antarctic multi-year snowfall analysis.

3.3. Antarctic multi-year snowfall analysis

3.3.1. Annual gridded snowfall pattern

Following the same method used for the mean annual snowfall rate difference spatial maps (Fig. 4), the mean 2C-SNOW snowfall rate over the OP was computed. Fig. 10 shows the results obtained for 2C-SNOW (Fig. 10a) and the corresponding ERA-I value (Fig. 10b). ERA-I 0.75°×0.75° spatial resolution 12-hourly snowfall field data (Dee et al., 2011) were interpolated to

the CloudSat-defined 1°×1.5° grid and summed over the OP. The total ERA-I accumulated snowfall was di- vided by 4.5 (years) to obtain the mean snowfall accumulation per year. The ERA-I yearly mean snowfall accumulations were then compared to the mean CPR-derived snowfall rates [mm year^{-1}].

The first distinguishing Fig. 10 feature is that the magnitude of the mean annual snowfall rate is very similar over continental Antarctica. The same similarity was found in Palerme et al. (2017), with a mean snowfall rate over the Antarctic continent of 172 mm year^{-1} obtained from CloudSat observations and 165 mm year^{-1} simulated by ERA-I. Moreover, 2C-SNOW also describes the precipitation pattern similarly to ERA-I, showing more coastal precipitation. This coastal maximum is very apparent on the western Antarctic Peninsula, with a clear maximum over the western tip of the Peninsula that was also observed by Turner et al. (2002) and Van Lipzig et al. (2004). Distinct snowfall minima are diagnosed by both datasets over the Ross and Ronne ice shelves. Relative maxima are found over the coastal and adjacent ocean areas around 60° E and between 110°E and 150°E in both datasets, although a clear difference in the magnitude exists. Such difference could be due to the different approach used to determine wet snow and mixed precipitation in ERA-I and 2C-SNOW, as well as to snow microphysics assumptions employed by each dataset.

These results highlight that CPR observations, even with lower native spatiotemporal sampling than ERA-I, produce similar mean annual snowfall patterns over Antarctica. Oceanic differences could be due to reduced CPR sampling at lower latitudes, but may also indicate Z-S or numerical model deficiencies for oceanic snowfall.

Fig. 11 shows the mean annual ERA-I and CPR snowfall scatterplot remapped on the 1°×1.5° grid and separated by surface type. The two datasets show elevated correlations (0.91), largely caused by high correlations for snowfall rates below 400 mm year^{-1} (0.90). For larger snowfall values, the satellite (model) retrievals generally overestimate (underestimate) mean annual snowfall rates compared to ERA-I (CloudSat).

Considering different surface types, the > 2000 m datasets have a correlation of 0.83, while the ocean datasets display higher correlations (0.86). The < 2000 m correlation between ERA-I and CPR, however, is lower (0.44) with increased variance. Reduced < 2000 m correlations could be caused by ground clutter over the coastal and escarpment regions. 2C-SNOW Z-S conversions may also need further refinement over Antarctic land surfaces. Additionally, the orographic effects on the precipitation production in Antarctic environments may not be cor- rectly considered in the

model. These complications are discussed further in Section 4.

3.3.2. *Instantaneous snowfall rate analysis*

For a deeper discussion of the impact of general surface type and topography on the gross characteristics of snowfall, we report the normalized distribution of instantaneous snowfall rate (with snowfall rate bins of 0.1 mm h^{-1}), as estimated by 2C-SNOW, for the three surfaces (Fig. 12). The normalization is made with respect to the total number of "snow" profiles, i.e., profiles with snowfall rate larger than 0.1 mm h^{-1}. The snowfall rate over the > 2000 m is very low, as > 99% of the CPR detected snow profiles are below 1 mm h^{-1}. It should be noted, though, that snow accumulation in this area is mainly due to small ice crystal sedimentation under clear skies (Bromwich, 1988; Knuth et al., 2010), likely associated with very low rates that are either too light for CPR detection or would not be considered as 2C- SNOW "snow probable" conditions with a CPR reflectivity exceeding −15 dBZ. Ocean and < 2000 m profiles show similar patterns, with maximum snowfall rate reaching the same value of 5 mm h^{-1} with a relative abundance of higher snowrates over < 2000 m (above 2 mm h^{-1}) with respect to ocean profiles, indicating the orographic enhancement effect of the Antarctic coastal and escarpment zones on precipitation intensity. The respective surface type mean snowfall rates are 5.9×10^{-2} mm h^{-1} (ocean), 3.2×10^{-2} mm h^{-1} (< 2000 m), and 4.2×10^{-3} mm h^{-1} (> 2000 m).

3.3.3 *2C-SNOW comparison with monthly ground observations*

The lack of a snowfall ground based measurement network over the Antarctic region represents a significant impediment to directly com- pare the CloudSat 2C-SNOW product with measured data. Moreover, harsh environments like Antarctica adversely affect typical instrument reliability and can create data quality issues that compound the scarcity of ground validation networks. Despite these difficulties, we qualitatively compare 2C-SNOW estimates with a limited dataset of five ground based Acoustic Depth Gauge (ADG) observations to investigate the feasibility of making gross monthly snow accumulation comparisons between spaceborne and ground-based assets. A monthly 2C- SNOW mean snowfall rate and ADG measurement comparison for the last 2 OP years is performed to provide a qualitative CPR snowfall detection assessment. This study uses ADG stations that were both quality controlled and contained a sufficiently long record of tempo- rally continuous data coincident with CPR-indicated snowing over- passes within a 10 km distance. These criteria limited the number of ADG observations available, and their delimited

spatial distribution (mainly over the Ross Sea ice shelf) unfortunately limits the representativeness of the ADG-CPR comparison.

Fig. 13 shows monthly ADG distance variation comparisons to the monthly mean snowfall rate [mm month^{-1}] in each CPR grid box containing the ADG stations. The majority of the months with CPR- derived monthly snowfall accumulations are associated with negative ADG monthly distance variations (i.e. increase of snow height), espe- cially for monthly snowfall rates exceeding 25 mm month^{-1}. In case of lower 2C-SNOW snow rates, the ADG distance variations (both positive and negative) are dominated by other mechanisms (Li and Pomeroy, 1997; Knuth et al., 2010). This trend does not apply to the maximum 2C-SNOW snowfall rate (~320 mm month^{-1}) in September 2009 and November 2010, whereby the corresponding ADG value indicates small negative and positive ADG distance variations, respectively. More re- search must be undertaken to understand this apparent discrepancy, although it must be noted that this aberration occurred in a relatively warm month that can experience ablation and snow compaction (Radok and Lile, 1977; Knuth et al., 2010).

Contingency tables are often employed in validation exercises that compare satellite and ground-based values (e.g., Puca et al., 2014). Under these circumstances, the ADG distance variation cannot be as- sumed as the "true" representation of snow accumulation from pre- cipitation (see Section 2.2). However, a contingency table analysis (Table 1) can provide a useful exercise to qualitatively evaluate the two independent accumulation estimates.

Hits are defined when months with negative ADG distance varia- tions (monthly snow accumulation) correspond to monthly CPR mean snowfall rates exceeding zero. Conversely, misses indicate estimated CPR snowfall rates equal to zero. Finally, false alarms are counted when positive CPR snowfall rates match with negative or zero ADG distance variations (snow accumulation decrease or no variation). After analyzing the 140 monthly CPR and ADG values in the dataset, it was discovered that 69% of grid boxes where the CPR detects precipitation correspond to increasing ADG snow accumulation, while 99% (75/76) of grid boxes with increasing ADG snow accumulation have an estimated CPR snowfall exceeding zero. Blowing snow is a large possible factor to explain discrepancies. For instance, the only case where an ADG snow accumulation increase does not correspond to estimated snowfall amount above zero could be due to a blowing snow episode. The most glaring discrepancy is related to the 34 cases where CPR estimates positive monthly snowfall rates, but the ADG does not measure a monthly accumulation. Blowing snow again play a role by trans- porting snow away from the ADG sites.

Many other mechanisms could also decrease the snowpack on a monthly basis, and these factors need to be studied further to determine the complex interplay between sur- face snow addition and removal by non-precipitation processes.

4. Summary and conclusions

CloudSat observations have enabled a new era of global snowfall monitoring, including critically important regions that were previously devoid of quantitative precipitation estimates, like a large fraction of the Antarctic land mass, ice sheets, and nearby oceanic regions. Numerous retrieval methodologies have been developed to provide CloudSat snowfall rate retrievals, and a scientific focal point of the current study illustrates systematic differences in snowfall rate estimates between various retrieval approaches over Antarctica and the Southern Ocean. After accounting for key algorithm differences in the Kulie and Bennartz (2009) with Hiley et al. (2011 - KBH) and 2C- SNOW-PROFILE (2C-SNOW) CloudSat snowfall retrievals, Antarctic and Southern Ocean snowfall estimate differences were isolated to the inherent reflectivity (Z) to snowfall rate (S) conversions used by each retrieval. The 2C-SNOW dynamic Z-S optimal estimation approach was deemed advantageous compared to the static KBH Z-S method, as the 2C-SNOW retrievals account for apparent systematic microphysical composition differences over varying Antarctic regions (< 2000 m versus > 2000 m versus ocean). 2C-SNOW mean annual snowfall rates were systematically higher than the KBH algorithm after algorithm differences were minimized. These differences were especially prominent over the Southern Ocean, Antarctic Peninsula, and coastal regions. Spatial algorithm annual snowfall rate differences were minimal over interior Antarctic regions that experience mostly light snowfall events. Similar to spatial algorithm differences, 2C-SNOW and KBH snowfall rate distributions displayed markedly different characteristics over a wide range of the snowfall rate spectrum, especially the ~0.5 to 4.5 mm h^{-1} range where the population of 2C-SNOW snowfall rates far exceeded KBH counts in the same range for the entire dataset, although distinct regional differences in snowfall rate distributions were noted (ocean versus < 2000 m versus > 2000 m). KBH sensitivity tests also highlighted algorithm assumptions that are seemingly detrimental to snowfall detection over this region. For instance, the KBH vertical reflectivity continuity test, near surface bin selection, and strict temperature thresholds are shown to drastically reduce the snowfall population, especially over-ocean regions that are prone to shallow convective snow as indicated by the ERA-Interim

dataset.

This study also provides derived Z-S relationships using 2C-SNOW snowfall rate retrievals and observed CloudSat radar reflectivity values. The derived Z-S relationship for all snowfall events southward of 60°S latitude is $Z = 10.9\ S^{1.3}$, but 2C-SNOW estimates different Z-S relationships over ocean ($Z = 8.2\ S^{1.3}$), < 2000 m ($Z = 6.7\ S^{1.4}$), and > 2000 m ($Z = 5.5\ S^{1.6}$), where < 2000 m and > 2000 m are differentiated by the 2000 m elevation above sea level threshold. By comparison, the static KBH-like Z-S relationship is $Z = 21.6\ S^{1.2}$. The 2C- SNOW Z-S relationships highlight underlying microphysical differences driven by ambient temperature and other environmental conditions that are included in the 2C-SNOW optimal estimation retrieval as a priori constraints. The Z-S relationships reported in this study can be utilized by, for instance, ground-based W-band radars employed in similar environments.

A multi-year 2C-SNOW mean annual snowfall analysis is also provided by this study over the Antarctic and Southern Ocean region. This observational analysis shows enhanced snowfall accumulations along the Antarctic coast and western tip of the Antarctic Peninsula, with a pronounced snowfall gradient from the coast to inland portions of the continent. Very low snowfall totals occur in Antarctica's interior sections. Pronounced snowfall minima also occur over the major ice shelves (e.g., Ross, Ronne) when compared to surrounding waters that experience transient ice formation. Comparisons with ERA-Interim (ERA-I) snowfall datasets show very similar spatial patterns. Distinct magnitude differences are observed mostly over ocean locations, where 2C-SNOW shows systematically higher average snowfall rates than ERAeI. The respective datasets are also highly correlated over ocean. The 2C-SNOW and ERA-I datasets exhibit good agreement over the > 2000 m, with elevated correlations and low random errors. < 2000 m comparisons have much lower correlations and higher variability, al- though < 2000 m estimates do not display strong systematic biases similar to over ocean. Over ocean comparisons might be affected by phase discrimination differences. Similarly, over < 2000 m comparisons are complicated by possible ground clutter in the 2C-SNOW dataset, even though stringent clutter mitigation techniques are employed to reduce its occurrence.

Two final analyses are offered in this study. First, 2C-SNOW snowfall rate distributions are partitioned by surface type (ocean versus < 2000 m versus > 2000 m). The respective snowfall rate distributions display markedly different characteristics, with evidence of < 2000 m enhancement producing a higher percentage of elevated snowfall rate values compared to ocean and > 2000 m. The > 2000 m snowfall rate distribution is skewed toward lower snowfall rate values, with very

few instances of elevated snowfall rates exceeding 1–2 mm h^{-1}. Second, a comparison between monthly 2C-SNOW and five ground based acoustic depth gauges (ADG) deployed in Antarctica is provided to demonstrate qualitative trends in snow accumulation between the respective data- sets. Most months with CPR-derived positive snowfall correspond to net monthly ADG accumulations, although considerable variability in the magnitudes of both respective datasets is associated with this analysis due to various complications (e.g., wind-driven horizontal snow transport affecting ADG statistics). While this ADG-CloudSat monthly comparison dataset is admittedly geographically restricted to the Ross Ice Shelf, it provides a possible pathway for further long-term analyses using a broader ADG network.

The results presented in this study provide a useful multi-year snowfall analysis for Antarctica and the Southern Ocean, building upon previous CloudSat and ERA-I research that has been undertaken in re- cent years. While the algorithm comparisons and sensitivity tests elucidate algorithm-specific assumptions and methodological differences that strongly influence snowfall detection and quantitative precipitation estimates, these results highlight the need for further ground or ocean based evaluation datasets in this region. There is a desperate need for robust ground based datasets to evaluate 2C-SNOW estimates. In particular, developing ground-based Z-S relationships using profiling radar and ground based snowfall rate estimates is a high priority task that must be undertaken to compare with CloudSat 2C-SNOW estimates, especially for the various environments highlighted in this study (ocean, < 2000 m, > 2000 m). While difficult to undertake, ground- based snow accumulation statistics to augment the rudimentary ADG analysis in this study are also needed using a variety of possible in situ measurements. Cloud microphysics observations to constrain a priori assumptions employed by 2C-SNOW algorithm are also needed, as the observations utilized in the 2C-SNOW algorithm may not be appropriate for Antarctic environments. Finally, extended over ocean observations are desired to verify CloudSat and ERA-I snowfall estimates, especially rain/snow phase discrimination and the need to validate 2C- SNOW microphysics and Z-S relationships that appear to be very different over oceanic environments.

Acknowledgments

References

Arthern, R.J., Winebrenner, D.P., Vaughan, D.G., 2006. Antarctic snow accumulation mapped using polarization of 4.3-cm wavelength microwave emission. J. Geophys. Res. 111, D06107. http://dx.doi.org/10.1029/2004JD005667.

Behrangi, A., Christensen, M., Richardson, M., Lebsock, M., Stephens, G., Huffman, G.J., Bolvin, D., Adler, R.F., Gardner, A., Lambrigtsen, B., Fetzer, E., 2016. Status of high- latitude precipitation estimates from observations and reanalyses. J. Geophys. Res. 121, 4468–4486. http://dx.doi.org/10.1002/2015JD024546.

Bindschadler, R., Choi, H., Shuman, C., Markus, T., 2005. Detecting and measuring new snow accumulation on ice sheets by satellite remote sensing. Remote Sens. Environ. 98, 388–402.

Boening, C., Lebsock, M., Landerer, F., Stephens, G., 2012. Snowfall-driven mass change on the East Antarctic ice sheet. Geophys. Res. Lett. 39, L21501. http://dx.doi.org/10.1029/2012GL053316.

Bromwich, D.H., 1988. Snowfall in high southern latitudes. Rev. Geophys. 26 (1), 149–168.

Bromwich, D.H., Guo, Z., Bai, L., Chen, Q.-S., 2004. Modeled Antarctic precipitation. Part I: Spatial and temporal variability. J. Clim. 17, 427–447.

Bromwich, D.H., Nicolas, J.P., Monaghan, A.J., 2011. An assessment of precipitation changes over Antarctica and the Southern Ocean since 1989 in contemporary global reanalysis. J. Clim. 24, 4189–4209.

Bromwich, D.H., Nicolas, J.P., Monaghan, A.J., Lazzara, M.A., Keller, L.M., Weidner, G.A., Wilson, A.B., 2013. Central West Antarctica among the most rapidly warming regions on

earth. Nat. Geosci. 6, 139–145. http://dx.doi.org/10.1038/ngeo1671.

Casella, D., Panegrossi, G., Sanò, P., Marra, A.C., Dietrich, S., Johnson, B.T., Kulie, M.S., 2017. Evaluation of the GPM-DPR snowfall detection capability: comparison with CloudSat-CPR. Atmos. Res. 197, 64–75. http://dx.doi.org/10.1016/j.atmosres.2017. 06.018.

Clem, K.R., Fogt, R.L., 2015. South Pacific circulation changes and their connection to the tropics and regional Antarctic warming in austral spring, 1979–2012. J. Geophys. Res. Atmos. 120, 2773–2792. http://dx.doi.org/10.1002/2014JD022940.

Cooper, S.J., Wood, N.B., L'Ecuyer, T.S., 2017. A variational technique to estimate snowfall rate from coincident radar, snowflake, and fall-speed observations. Atmos. Meas. Tech. 10, 2557–2571. http://dx.doi.org/10.5194/amt-10-2557-2017.

Dee, D.P., Uppala, S.M., Simmons, A.J., Berrisford, P., Poli, P., Kobayashi, S., Andrae, U., Balmaseda, M.A., Balsamo, G., Bauer, P., Bechtold, P., Beljaars, A.C.M., van de Berg, L., Bidlot, J., Bormann, N., Delsol, C., Dragani, R., Fuentes, M., Geer, A.J., Haimberger, L., Healy, S.B., Hersbach, H., Hólm, E.V., Isaksen, L., Kållberg, P., Köhler, M., Matricardi, M., McNally, A.P., Monge-Sanz, B.M., Morcrette, J.-J., Park, B.-K., Peubey, C., de Rosnay, P., Tavolato, C., Thépaut, J.-N., Vitart, F., 2011. The ERA-interim reanalysis: configuration and performance of the data assimilation system. Quart. J. Roy. Meteorol. Soc. 137 (656), 553–597. http://dx.doi.org/10. 1002/qj.828.

Eisen, O., Frezzotti, M., Genthon, C., Isaksson, E., Magand, O., van den Broeke, M.R., Dixon, D.A., Ekaykin, A., Holmlund, P., Kameda, T., Karlöf, L., Kaspari, S., Lipenkov, V.Y., Oerter, H., Takahashi, S., Vaughan, D.G., 2008. Ground-based measurements of spatial and temporal variability of snow accumulation in East Antarctica. Rev. Geophys. 46 (2), RG2001. http://dx.doi.org/10.1029/2006RG000218.

Field, P.R., Hogan, R.J., Brown, P.R.A., Illingworth, A.J., Choularton, T.W., Cotton, R.J., 2005. Parametrization of ice-particle size distributions for mid-latitude stratiform cloud. Quart. J. Roy. Meteorol. Soc. 131, 1997–2017. http://dx.doi.org/10.1256/qj. 04.134.

Genthon, C., Krinner, G., 2001. The Antarctic surface mass balance and systematic biases in general circulation models. J. Geophys. Res. 106 (D18), 20,653–20,664.

Gong, J., Wu, D.L., 2017. Microphysical properties of frozen particles inferred from Global Precipitation Measurement (GPM) Microwave Imager (GMI) polarimetric measurements.

Atmos. Chem. Phys. 17, 2751–2757. http://dx.doi.org/10.5194/acp- 17-2741-2017.

Gorodetskaya, I.V., Tsukernik, M., Claes, K., Ralph, M.F., Neff, W.D., Van Lipzig, N.P.M., 2014. The role of atmospheric rivers in anomalous snow accumulation in East Antarctica. Geophys. Res. Lett. 41, 6199–6206. http://dx.doi.org/10.1002/ 2014GL060881.

Gorodetskaya, I.V., Kneifel, S., Maahn, M., Van Tricht, K., Schween, J.H., Crewell, S., Van Lipzig, N.P.M., 2015. Cloud and precipitation properties from ground-based remote sensing instruments in East Antarctica. Cryosphere 9, 285–304. http://dx.doi.org/10. 5194/tc-9-285-2015.

Grazioli, J., Genthon, C., Boudevillain, B., Duran-Alarcon, C., Del Guasta, M., Madeleine, J.-B., Berne, A., 2017. Measurements of precipitation in Dumont d'Urville, Adélie Land, East Antarctica. Cryosphere 11, 181–1797. http://dx.doi.org/10.5194/tc-11- 1797-2017.

Guo, Z., Bromwich, D.H., Cassano, J.J., 2003. Evaluation of polar MM5 simulations of Antarctic atmospheric circulation. Mon. Weather Rev. 131, 384–411. http://dx.doi. org/10.1175/1520-0493.

Haynes, J., L'Ecuyer, T.S., Stephens, G., Miller, S., Mitrescu, C., Tanelli, S., 2009. Rainfall retrieval over the ocean with spaceborne W-band radar. J. Geophys. Res. 114. http:// dx.doi.org/10.1029/2008JD009973.

Hiley, M.J., Kulie, M.S., Bennartz, R., 2011. Uncertainties in CloudSat snowfall retrievals. J. Appl. Meteorol. Climatol. 50, 399–418.

Hong, G., 2007. Radar backscattering properties of nonspherical ice crystals at 94 GHz. J. Geophys. Res. 112, D22203. http://dx.doi.org/10.1029/2007JD008839.

Hou, A.Y., Kakar, R.K., Neeck, S., Azarbarzin, A.A., Kummerow, C.D., Kojima, M., Oki, R., Nakamura, K., Iguchi, T., 2014. The global precipitation measurement mission. Bull. Amer. Meteorol. Soc. 95, 701–722. http://dx.doi.org/10.1175/BAMS-D-13-00164.1.

Hudak, D., Rodriguez, P., Donaldson, N., 2008. Validation of the CloudSat precipitation occurrence algorithm using the Canadian C band radar network. J. Geophys. Res. 113. http://dx.doi.org/10.1029/2008JD009992.

Huffman, G., Bolvin, D., Nelkin, E., Wolff, D., Adler, R., Gu, G., Hong, Y., Bowman, K., Stocker, E., 2007. The TRMM Multisatellite Precipitation Analysis (TMPA): quasi- global, multiyear, combined-sensor precipitation estimates at fine scales. J.

Hydrometeorol. 8, 38–55. http://dx.doi.org/10.1175/JHM560.1.

Johnson, B.T., Petty, G.W., Skofronick-Jackson, G., 2012. Microwave properties of ice- phase hydrometeors for radar and radiometers: sensitivity to model assumptions. J. Appl. Meteorol. Climatol. 51 (12), 2152–2171. http://dx.doi.org/10.1175/JAMC-D-11-0138.1.

Knuth, S.L., Tripoli, G.J., Thom, J.E., Weidner, G., 2010. The influence of blowing snow and precipitation on SSH change across the Ross ice shelf and Ross Sea regions of Antarctica. J. Appl. Meteorol. Climatol. 49, 1306–1321.

Kongoli, C., Meng, H., Dong, J., Ferraro, R., 2015. A snowfall detection algorithm over land utilizing high-frequency passive microwave measurements-application to ATMS. J. Geophys. Res. Atmos. 120, 1918–1932. http://dx.doi.org/10.1002/ 2014JD022427.

Kulie, M.S., Bennartz, R., 2009. Utilizing space-borne radars to retrieve dry snowfall. J. Appl. Meteorol. 48, 2564–2580.

Kulie, M.S., Milani, L., 2018. Seasonal variability of shallow cumuliform snowfall: a CloudSat perspective. Q. J. R. Meteorol. Soc. http://dx.doi.org/10.1002/qj.3222.

Kulie, M.S., Bennartz, R., Greenwald, T., Chen, Y., Weng, F., 2010. Uncertainties in mi- crowave optical properties of frozen precipitation: implications for remote sensing and data assimilation. J. Atmos. Sci. 67, 3471–3487.

Kulie, M.S., Milani, L., Wood, N.B., Tushaus, S., Bennartz, R., L'Ecuyer, T.S., 2016. A shallow cumuliform snowfall census using spaceborne radar. J. Hydrometeorol. 17, 1261–1279.

Laviola, S., Levizzani, V., 2011. The 183-WSL fast rainrate retrieval algorithm. Part I: retrieval design. Atmos. Res. 99, 443–461.

Li, L., Pomeroy, J.W., 1997. Probability of occurrence of blowing snow. J. Geophys. Res. 102, 21955–21964.

Liu, G., 2008. Deriving snow cloud characteristics from CloudSat observations. J. Geophys. Res. 113. http://dx.doi.org/10.1029/2007JD009766.

Lubin, D., Massom, R., 2006. Polar Remote Sensing. Volume I: Atmosphere and Oceans Springer-Verlag, Berlin Heidelberg. http://dx.doi.org/10.1007/3-540-30785-0.

Maahn, M., Burgard, C., Crewell, S., Gorodetskaya, I.V., Kneifel, S., Lhermitte, S., Van Tricht, K., van Lipzig, N.P.M., 2014. How does the spaceborne radar blind zone affect derived surface snowfall statistics in polar regions? J. Geophys. Res. Atmos. 119 (13), 604–613,620.

Mace, G., 2007. Level 2 GEOPROF Product Process Description and Interface Control

Document Algorithm Version 5.3. http://www.cloudsat.cira.colostate.edu/sites/default/files/products/files/2B-GEOPROF_PDICD.P_R04.20070628.pdf, Accessed date: 3 December 2018.

Marchand, R., Mace, G.G., Ackerman, T., Stephens, G., 2008. Hydrometeor Detection Using Cloudsat—An Earth-Orbiting 94-GHz Cloud Radar. J. Atmos. Oceanic Technol. 25, 519–533. http://dx.doi.org/10.1175/2007JTECHA1006.1.

Matrosov, S.Y., Battaglia, A., 2009. Influence of multiple scattering on CloudSat mea- surements in snow: a model study. Geophys. Res. Lett. 36, L12806. http://dx.doi.org/10.1029/2009GL038704.

Matrosov, S.Y., Shupe, M.D., Djalalova, I.V., 2008. Snowfall retrievals using millimeter-wavelenght cloud radars. J. Appl. Meteorol. Climatol. 47, 769–777.

Munchak, S.J., Skofronick-Jackson, G., 2013. Evaluation of precipitation detection over various surfaces from passive microwave imagers and sounders. Atmos. Res. 131, 81–94. http://dx.doi.org/10.1016/j.atmosres.2012.10.011.

Nicolas, J.P., Bromwich, D.H., 2014. New reconstruction of Antarctic near-surface tem- peratures: multidecadal trends and reliability of global reanalyses. J. Clim. 27, 8070–8093. http://dx.doi.org/10.1175/JCLI-D-13-00733.1.

Palerme, C., Kay, J.E., Genthon, C., L'Ecuyer, T.S., Wood, N.B., Claud, C., 2014. How much snow falls on the Antarctic ice sheet. Cryosphere 8, 1279–1304. http://dx.doi. org/10.5194/tcd-8-1279-2014.

Palerme, C., Claud, C., Dufour, A., Genthon, C., Wood, N.B., L'Ecuyer, T.S., 2017. Evaluation of Antarctic snowfall in global meteorological reanalyses. Atmos. Res. 190, 104–112. http://dx.doi.org/10.1016/j.atmosres.2017.02.015.

Panegrossi, G., Rysman, J.-F., Casella, D., Marra, A.C., Sanò, P., Kulie, M.S., 2017. CloudSat-based assessment of GPM microwave imager snowfall observation cap- abilities. Remote Sens. 9, 1263. http://dx.doi.org/10.3390/rs9121263.

Partain, P., 2007. Cloudsat ECMWF-AUX Auxiliary Data Process Description and Interface Control Document, Algorithm Version 5.2. http://www.cloudsat.cira.colostate.edu/sites/default/files/products/files/ECMWF-AUX_PDICD.P_R04.20070718.pdf, Accessed date: 3 December 2018.

Puca, S., Porcu, F., Rinollo, A., Vulpiani, G., Baguis, P., Balabanova, S., Campione, E., Ertürk, A., Gabellani, S., Iwanski, R., Jurašek, M., Kaňák, J., Kerényi, J., Koshinchanov, G.,

Kozinarova, G., Krahe, P., Lapeta, B., Lábó, E., Milani, L., Okon, L., Öztopal, A., Pagliara, P., Pignone, F., Rachimow, C., Rebora, N., Roulin, E., Sönmez, I., Toniazzo, A., Biron, D., Casella, D., Cattani, E., Dietrich, S., Di Paola, F., Laviola, S., Levizzani, V., Melfi, D., Mugnai, A., Panegrossi, G., Petracca, M., Sanò, P., Zauli, F., Rosci, P., De Leonibus, L., Agosta, E., Gattari, F., 2014. The validation service of the hydrological SAF geostationary and polar satellite precipitation products. Nat. Hazards Earth Syst. Sci. 14, 871–889. http://dx.doi.org/10.5194/nhess-14-871- 2014.

Radok, U., Lile, R.C., 1977. A year of snow accumulation at Plateau Station, meteor- ological studies at Plateau Station. Antarctica Antarctic Res. Ser. 25, 17–26.

Skofronick-Jackson, G., Johnson, B.T., 2011. Thresholds of detection for falling snow from satellite-borne active and passive sensors. In: Proc. IEEE Int. Conf. on Geoscience and Remote Sensing Symp, Vancouver, pp. 2637–2640. http://dx.doi.org/10.1109/IGARSS.2011.6049744.

Souverijns, N., Gossart, A., Lhermitte, S., Gorodetskaya, I.V., Kneifel, S., Maahn, M., Bliven, F.L., van Lipzig, N.P.M., 2017. Estimating radar reflectivity - snowfall rate relationships and their uncertainties over Antarctica by combining disdrometer and radar observations. Atmos. Res. 196, 211–223.

Stephens, G.L., Vane, D.G., Boain, R.J., Mace, G.G., Sassen, K., Wang, Z., Illingworth, A.J., O'Connor, E.J., Rossow, W.B., Durden, S.L., Miller, S.D., Austin, R.T., Benedetti, A., Mitrescu, C., The CloudSat Science Team, 2002. The CloudSat Mission and the A- Train. Bull. Am. Meteorol. Soc. 83 (12), 1771–1790.

Stephens, G.L., Vane, D.G., Tanelli, S., Im, E., Durden, S., Rokey, M., Reinke, D., Partain, P., Mace, G.G., Austin, R., L'Ecuyer, T.S., Haynes, J., Lebsock, M., Suzuki, K., Waliser, D., Wu, D., Kay, J., Gettelman, A., Wang, Z., Marchand, R., 2008. CloudSat mission: Performance and early science after the first year of operation. J. Geophys. Res. 113, D00A18. http://dx.doi.org/10.1029/2008JD009982.

Surussavadee, C., Staelin, D.H., 2009. Satellite retrievals of Arctic and Equatorial rain and snowfall rates using millimeter wavelengths. IEEE Trans. Geosci. Remote Sens. 47, 3697–3707. http://dx.doi.org/10.1109/TGRS.2009.2029093.

Tanelli, S., Durden, S.L., Im, E., Pak, K.S., Reinke, D.G., Partain, P., Haynes, J.M., Marchand, R.T., 2008. CloudSat's cloud profiling radar after two years in orbit: performance, calibration, and processing. IEEE Trans. Geosci. Remote Sens. 46, 3560–3573. http://dx.doi.org/10.1109/TGRS.2008.2002030.

Tapiador, F.J., Navarro, A., Levizzani, V., García-Ortega, E., Huffman, G.J., Kidd, C., Kucera, P.A., Kummerow, C.D., Masunaga, H., Petersen, W.A., Roca, R., Sánchez, J.- L., Tao, W.-K., Turk, F.J., 2017. Global precipitation measurements for validating climate models. Atmos. Res. 197, 1–20. http://dx.doi.org/10.1016/j.atmosres.2017. 06.021.

Turner, J., Lachlan-Cope, T.A., Marshall, G.J., Morris, E.M., Mulvaney, R., Winter, W., 2002. Spatial variability of Antarctic Peninsula net surface mass balance. J. Geophys. Res. 107 AAC 4–1 – AAC 4–18. https://doi.org/10.1029/2001JD000755.

Van Lipzig, N.P.M., King, J.C., Lachlan-Cope, T.a., Van den Broeke, M.R., 2004. Precipitation, sublimation, and snow drift in the Antarctic peninsula region from a regional atmospheric model. J. Geophys. Res. Atmos. 109 (24), 1–16. http://dx.doi. org/10.1029/2004JD004701.

Van Wessem, J.M., Reijmer, C., Morlighem, M., Mouginot, J., Rignot, E., Medley, B., Joughin, I., Wouters, B., Depoorter, M.A., Bamber, J.L., Lenaerts, J.T.M., Van De Berg, W.J., Van Den Broeke, M.R., Van Meijgaard, E., 2014. Improved representation of East Antarctic surface mass balance in a regional atmospheric climate model. J. Glaciol. 60 (222), 761–770. http://dx.doi.org/10.3189/2014JoG14J051.

Wood, N.B., L'Ecuyer, T.S., Vane, D.G., Stephens, G.L., Partain, P., 2013. Level 2C Snow-Profile Process Description and Interface Control Document, Algorithm Version P R04. http://www.cloudsat.cira.colostate.edu/sites/default/files/products/files/2C-SNOW-PROFILE_PDICD.P_R04.20130210.pdf, Accessed date: 3 December 2018.

You, Y., Wang, N.-Y., Ferraro, R., Rudlosky, S., 2017. Quantifying the snowfall detection performance of the GPM microwave imager channels over land. J. Hydrometeorol. 18, 729–751. http://dx.doi.org/10.1175/JHM-D-16-0190.1.

Tables

Table 1
Contingency table for monthly mean snowfall rate estimated by 2C-SNOW product and
ADG monthly distance variations (distance variation < 0 corresponds to an increase of snow
accumulation, distance variation ≥0 corresponds to a decrease or no variation of snow
accumulation).

	Monthly mean snowfall rate $>$ 0	Monthly mean snowfall rate $=$ 0
Distance variation <0	75	1
Distance variation ≥0	34	6

Figures
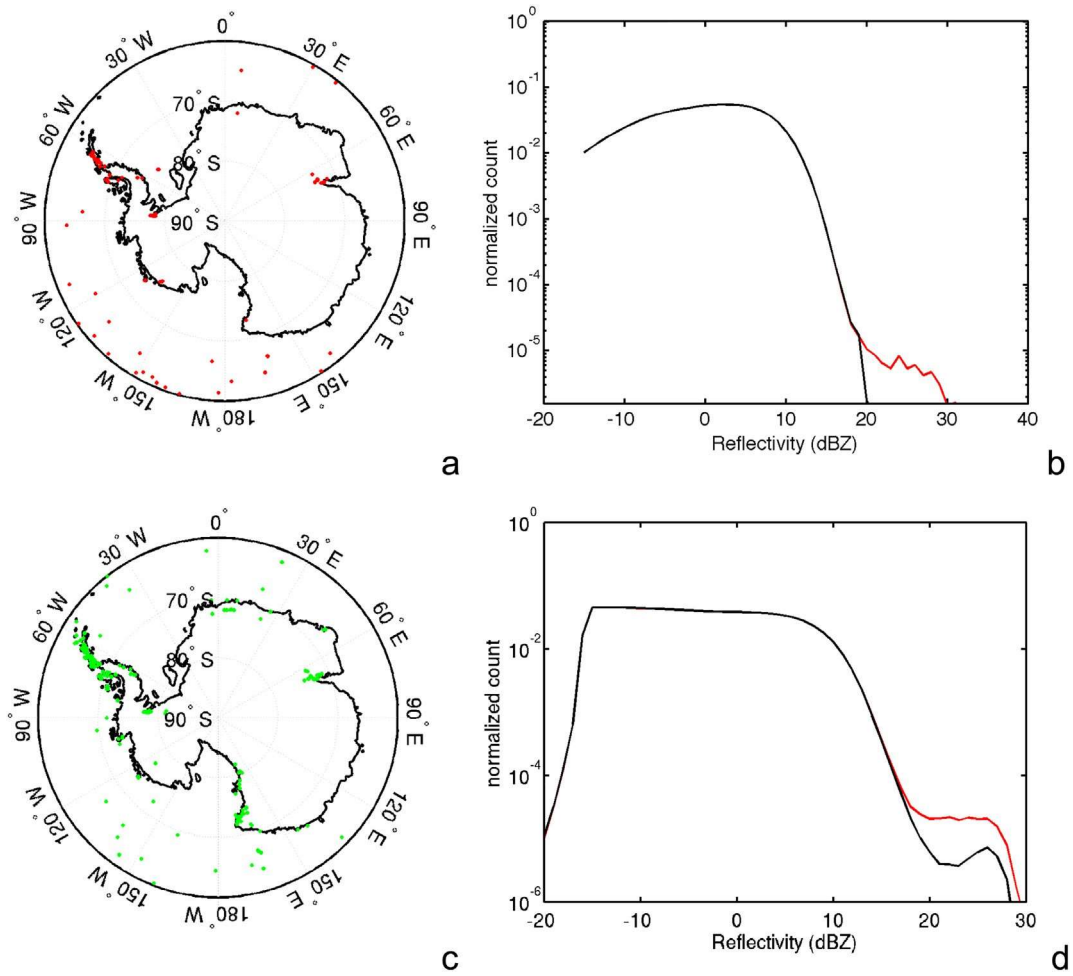
Fig. 1. a) Map showing the location of T ≤ 0 °C profiles flagged as ground clutter for KBH (red dots). b) Normalized distribution of the reflectivity corrected for ground clutter contamination (black line) calculated either for the 6th or the 8th bin (in case Z at the 6th bin exceeding 20 dBZ). Normalized distribution of the only 6th bin Z exceeding 20 dBZ is also shown (red line). c) T ≤ 0 °C profiles flagged as ground clutter for 2C-SNOW (green dots). d) Normalized distribution of the NSB reflectivity (black line) used by 2C-SNOW for the snowfall rate estimate. The normalized distribution of the profiles affected by ground clutter (see text for details) is also shown (red line). (For interpretation of the references to colour in this figure legend, the reader is referred to the web version of this article.)
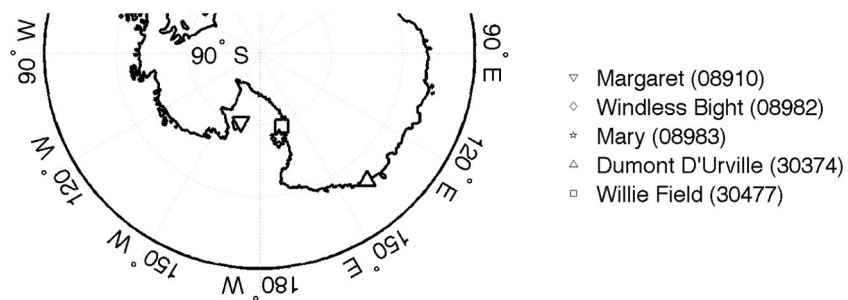
Fig. 2. Map showing the location of the 5 ADG
stations considered in this study.
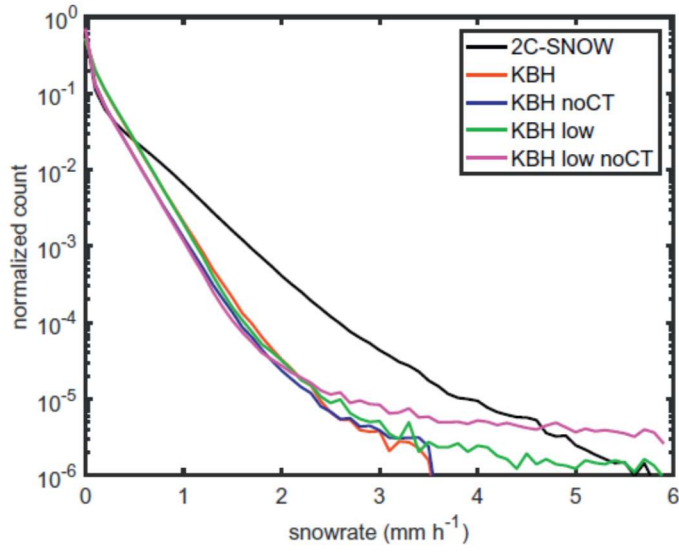
Fig. 3. Normalized distribution of 2C-SNOW (black line), KBH original (red line), KBH without the CT requirement (blue line), KBH applied to the same NSB as 2C-SNOW (green line), KBH without CT and applied to the same NSB as 2C-SNOW (pink line). (For interpretation of the references to colour in this figure legend, the reader is referred to the web version of this article.)
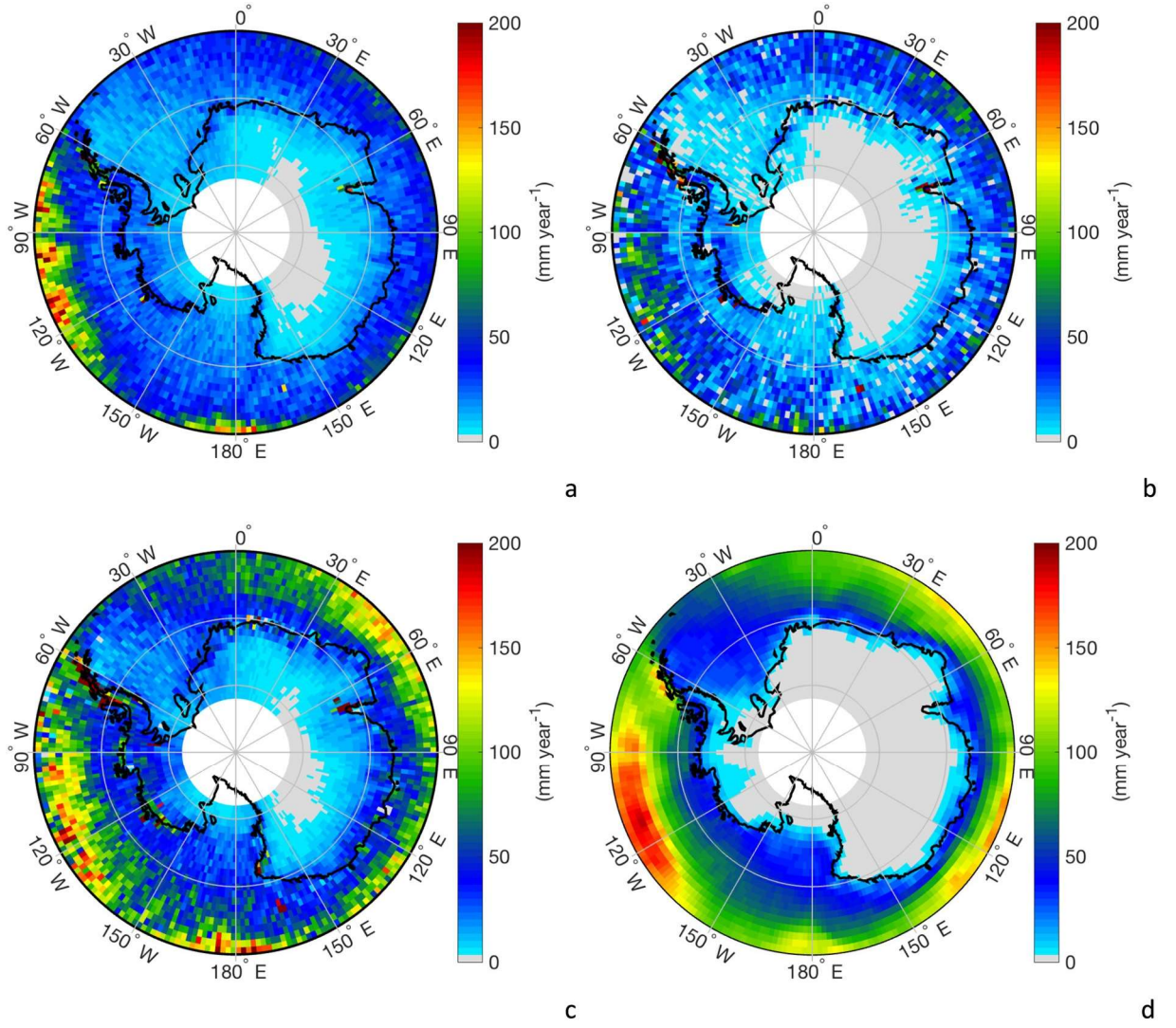
Fig. 4. Mean snowfall rate difference between: a) the original KBH NSB without vertical CT requirement, and with vertical CT requirement; b) the lowered KBH NSB and the original KBH NSB, both with CT applied; c) the lowered KBH NSB with no CT and the original KBH; d) ECMWF ERA-I reanalysis mean cumulated snowfall per year for convective snowfall.
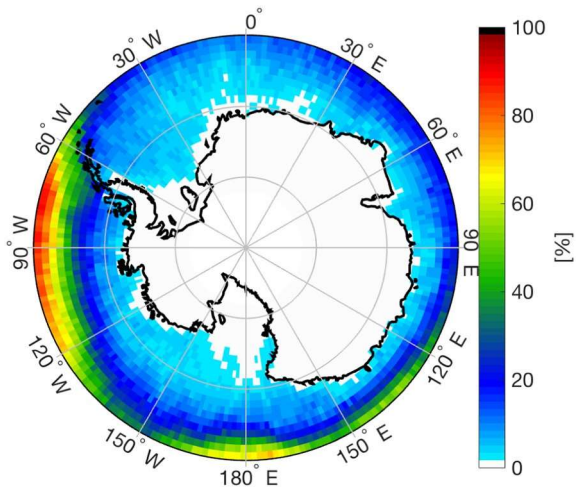
Fig. 5. Frequency of CloudSat observations associated with near-surface tem- perature exceeding 0 °C compared to the total number of CloudSat observations.
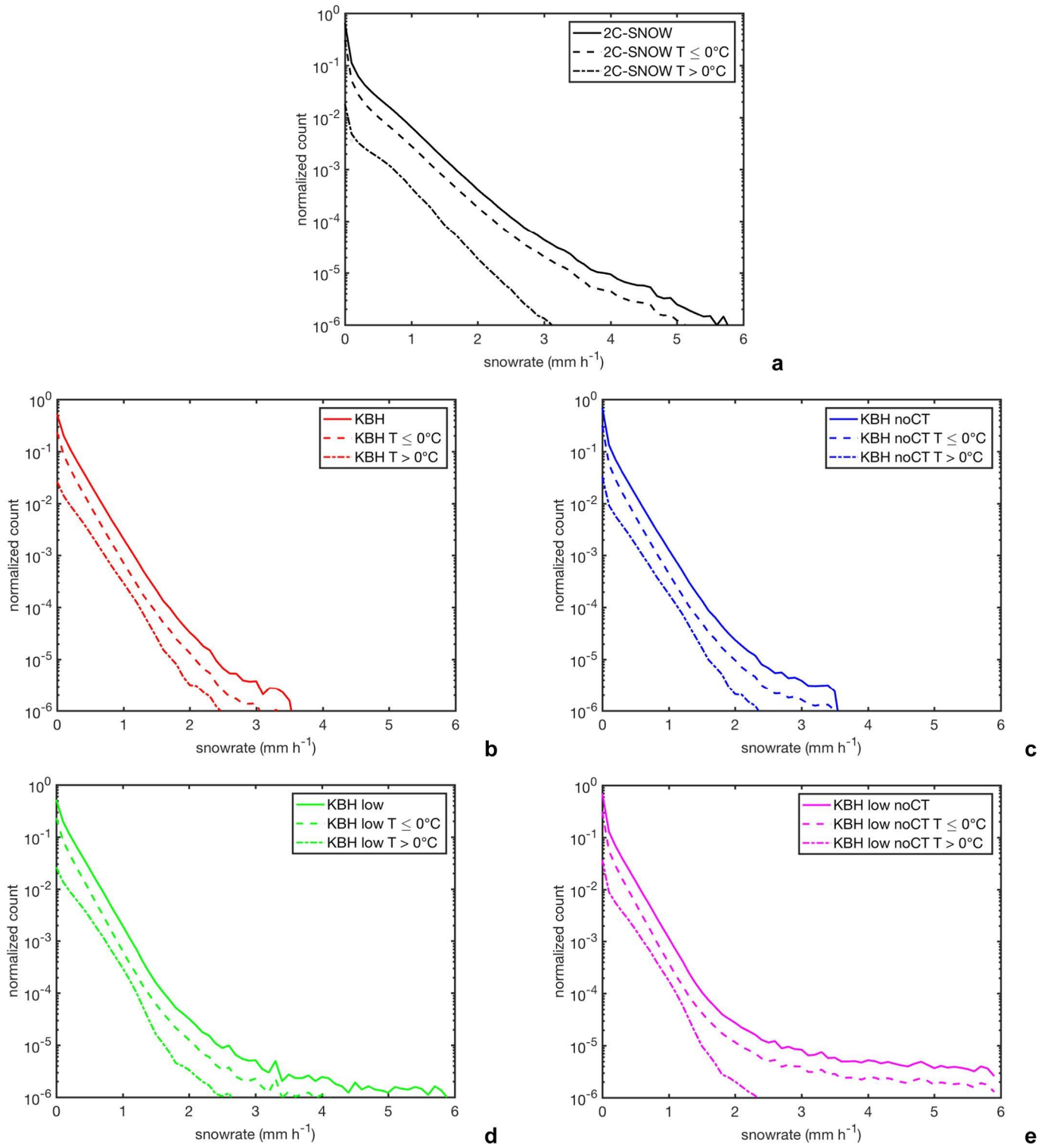
Fig. 6. Temperature filtered snowfall rate normalized distribution. a) 2C-SNOW, b) the original KBH; c) KBH NSB without CT requirement; d) lowered KBH NSB with CT applied d) lowered KBH NSB without CT requirement.
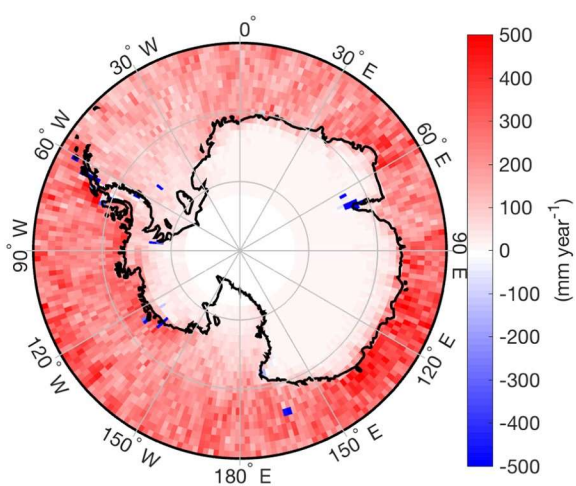
Fig. 7. Difference between 2C-SNOW mean snowfall rate and KBH modified (lower NSB without CT) snowrates for T ≤ 0 °C. Both algorithms therefore use the same NSB and temperature thresholds for this analysis.
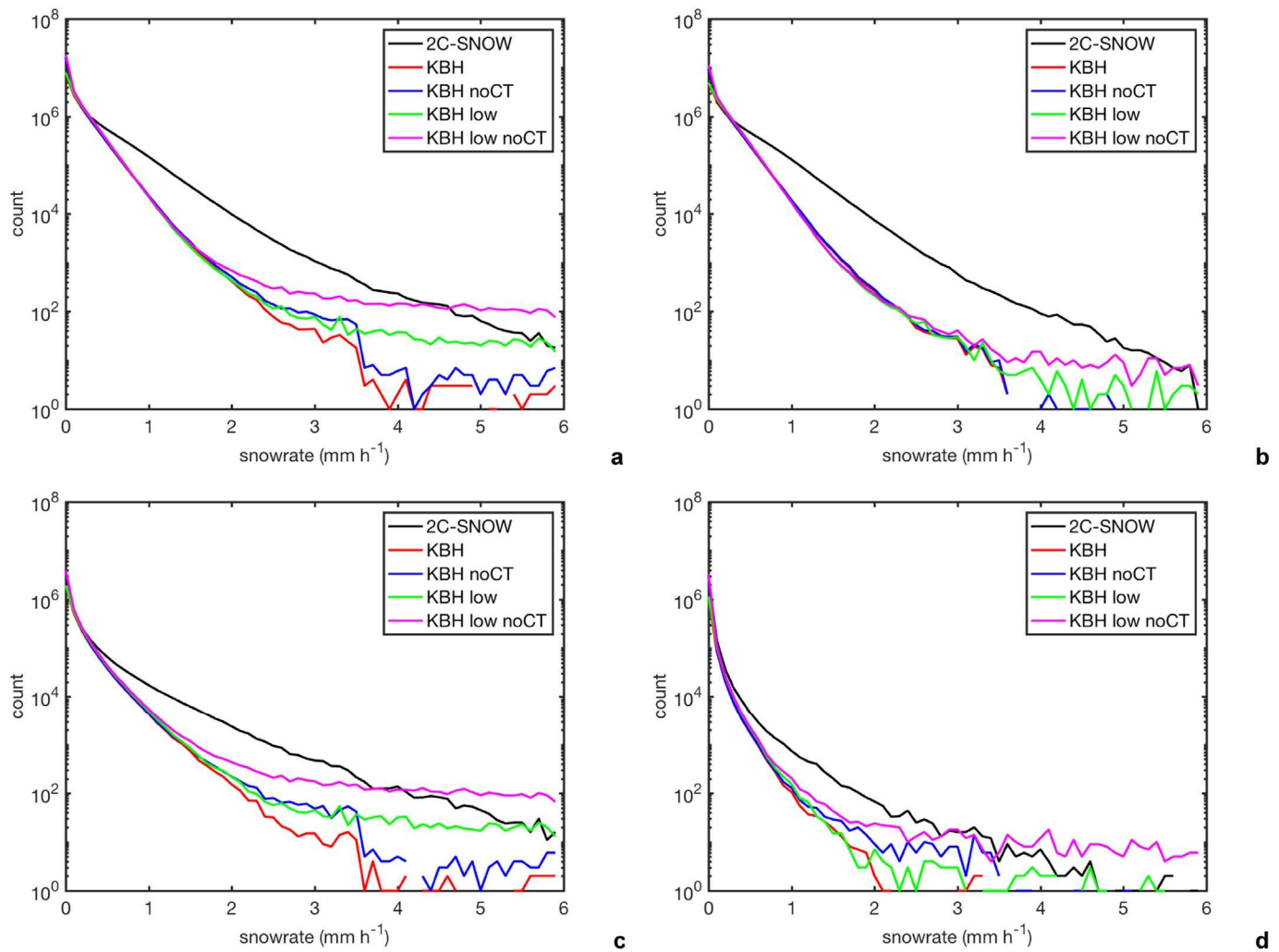
Fig. 8. Total number of snowfall counts (not normalized) associated with T ≤ 0 °C for a) all snow cases, b) ocean, c) < 2000 m, and d) > 2000 m. In each panel 2C- SNOW (black), the original KBH (red), KBH without CT requirement (blue), lowered KBH NSB with CT requirement (green), and lowered KBH NSB without CT requirement (pink) are shown. (For interpretation of the references to colour in this figure legend, the reader is referred to the web version of this article.)
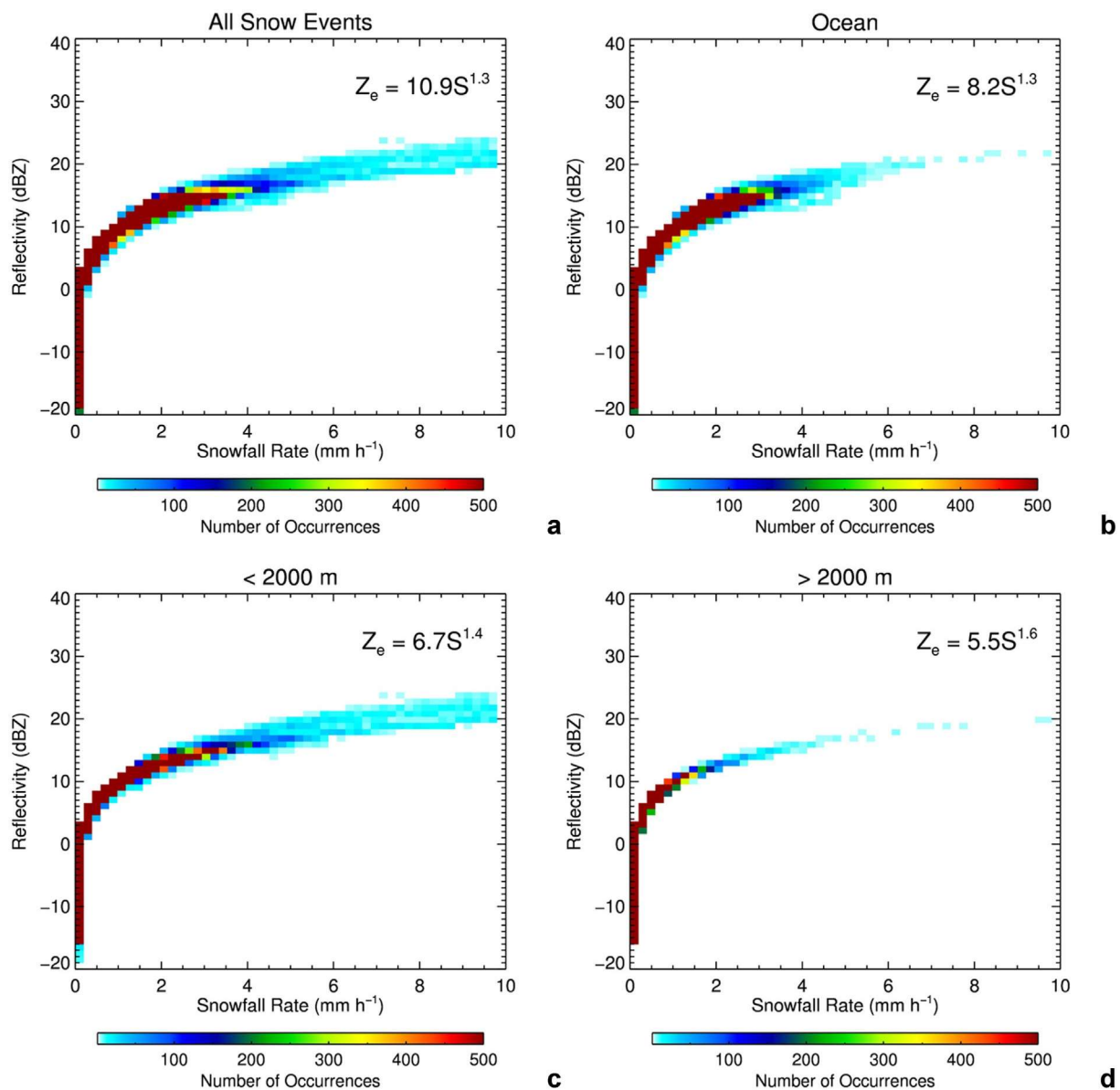
Fig. 9. Two-dimensional density snowfall rate [mm h^{-1}] and radar reflectivity [dBZ] scatterplots for T $\leq$ 0 °C profiles a) all profiles b) ocean c) < 2000 m d) > 2000 m.
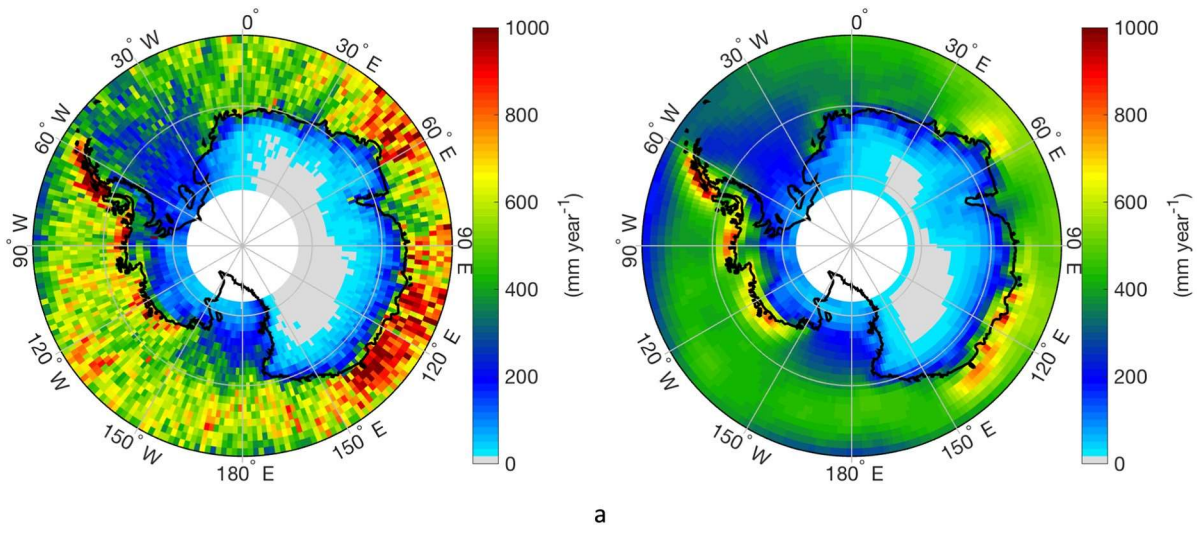
Fig. 10. a) 2C-SNOW mean annual snowfall rate, b) ERA-I mean
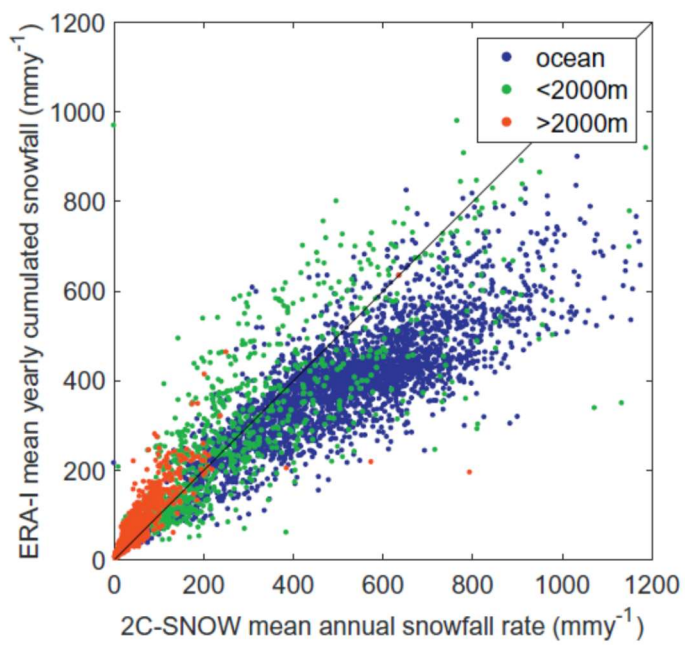yearly cumulated snowfall over the considered OP.

Fig. 11. ERA-I mean yearly cumulated snowfall vs. 2C-SNOW mean annual snowfall rate for three surface classes ocean, <2000 m, >2000 m.
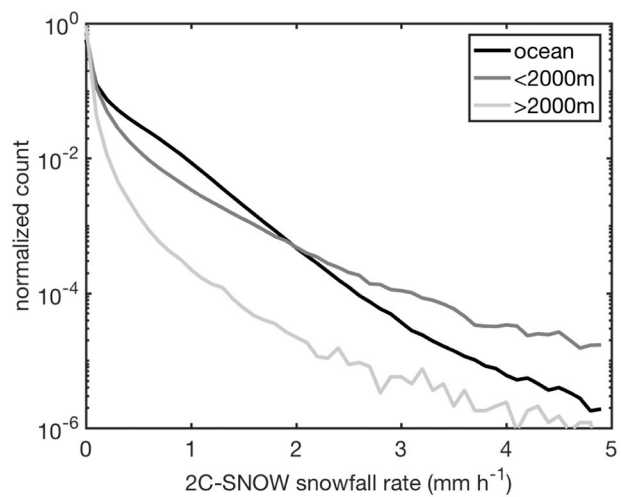
Fig. 12. Normalized counts of the 2C-SNOW instantaneous snowfall rate for the three surface type classes over the considered OP.
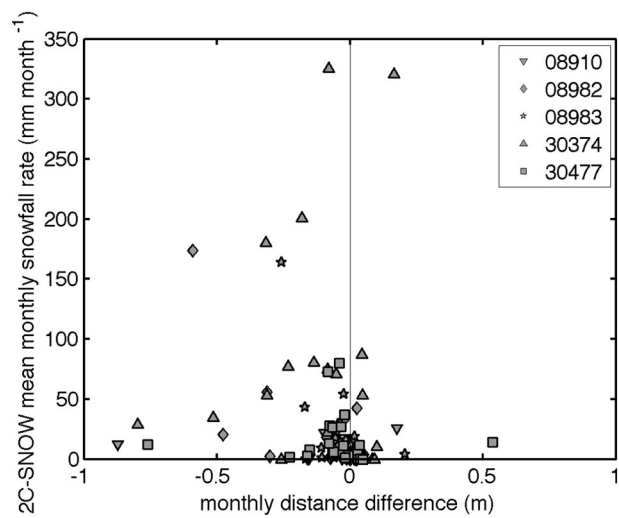
Fig. 13. CPR estimated mean monthly snowfall rate as a function of the monthly distance differences for the 5 ADG stations. Symbols refer to the stations as in Fig. 2.